Int. J. Solids Structures Vol. 30, No. 2, pp. 225–235, 1993
Printed in Great Britain.

0020–7683/93 $5.00+ .00

THERMO-ELASTO-VISCOPLASTIC DEFORMATION OF POLYMERIC BARS UNDER TENSION

YOSHIHIRO TOMITA and KENICHI HAYASHI
Faculty of Engineering, Kobe University, Rokkodai, Nada, Kobe 657, Japan

(*Received* 3 *October* 1991; *in revised form* 19 *June* 1992)

Abstract—The thermocoupled neck propagation behavior of circular cylindrical bars under tension has been investigated. These bars have a relatively low strain rate sensitivity and comply with a thermo-elasto-viscoplastic constitutive equation. Attention has been given to deformations with strain rate in the range of 0.0002–2 s^{-1} under isothermal, conductive and adiabatic conditions. A full axisymmetric finite element analysis of the velocity and temperature fields has clarified the effects of the deformation rate, material strain rate sensitivity and the thermal conductivity on neck propagation, including nonsteady-state deformation.

1. INTRODUCTION

The mechanical aspects of instability propagation in polymeric materials have recently received much attention. Hutchinson and Neale (1983) and Chater and Hutchinson (1984) investigated neck propagation of tension blocks, bulge propagation in long cylindrical balloons and buckle propagation of tubes under lateral pressure in terms of simple one-dimensional analysis. Hutchinson and Neale (1983) presented an approximate three-dimensional analysis of neck propagation along a round tensile bar under a steady-state condition. In further studies, full finite-element analyses for a solid circular bar (Neale and Tugcu, 1985) and plane strain block (Fager and Bassani, 1986; Tugcu and Neale, 1987a) have been conducted. Kyriakides *et al.* (1984) and Kyriakides (1986) discussed a buckle propagation. Tomita *et al.* (1990) investigated quasi-static neck and bulge propagation with respect to circumferential and axial directions, respectively, in cylinders under internal pressure.

However, due to the strain rate and temperature sensitivity of the material, the instability propagation behavior manifested different features associated with the boundary conditions applied. In subsequent studies, the effects of strain rate sensitivity (Tugcu and Neale, 1987a, b, 1988), the temperature dependency (Tugcu and Neale, 1990a; Tugcu *et al.*, 1991) and kinematic hardening (Tugcu and Neale, 1987a) on neck propagation behavior have been investigated. Tugcu and Neale (1987a) and Tugcu *et al.* (1991) were involved in the approximate steady-state analysis of axisymmetric fibers and plane strain films, respectively. Yet, details of thermo-elasto-viscoplastic neck propagation, including nonsteady-state deformation, are still open to investigation.

In this study, the thermo-elasto-viscoplastic deformation behavior of circular cylindrical bars subjected to uniaxial tension with different speeds has been investigated by a full axisymmetric finite-element method incorporating velocity and temperature field, and the characteristics of the deformation behavior have been clarified.

2. CONSTITUTIVE EQUATION

The temperature-dependent polymeric deformation behavior obtained experimentally (Itoh *et al.*, 1980) has been approximately modeled by a slightly modified uniaxial stress–strain relation by Fager and Bassani (1986):

$$\sigma_0 = \begin{cases} E\varepsilon & (\varepsilon \leqslant \varepsilon_y), \\ \mu(\varepsilon-\varepsilon_a)^N & (\varepsilon_y \leqslant \varepsilon \leqslant \varepsilon_L), \\ \beta \exp\{M(\varepsilon-\varepsilon_b)^2\} & (\varepsilon_L \leqslant \varepsilon). \end{cases} \tag{1}$$

In eqn (1) we take E, N, ε_a, ε_b, ε_y and ε_L as the independent material constants and impose a continuity requirement on the stress σ at $\varepsilon = \varepsilon_y$ and $\varepsilon = \varepsilon_L$, as well as continuity of the tangent modulus $d\sigma/d\varepsilon$ at $\varepsilon = \varepsilon_L$. This gives

$$\mu = E\varepsilon_y/(\varepsilon_y-\varepsilon_a)^N,$$
$$M = N/\{2(\varepsilon_L-\varepsilon_b)(\varepsilon_L-\varepsilon_a)\}, \quad \beta = \mu(\varepsilon_L-\varepsilon_a)^N/\exp\{M(\varepsilon_L-\varepsilon_b)^2\}. \tag{2}$$

Figure 1(a) shows the uniaxial stress–natural strain relations for different temperatures which were originally obtained by Itoh *et al.* (1980) and modeled by eqn (1), and Fig. 1(b) depicts the temperature dependency of the material parameters. The concrete form of Young's modulus E will be given at the end of Section 3. To account for the material strain rate sensitivity, the uniaxial stress–natural strain relation (1) is simply generalized as follows:

$$\sigma = \sigma_0(1+\dot{\varepsilon}/\dot{\varepsilon}_y)^m, \tag{3}$$

where $\dot{\varepsilon}$ is the natural strain rate, σ_0 is defined by eqn (1), $\dot{\varepsilon}_y$ is the material constant, and m is the strain rate sensitivity exponent. When either $\dot{\varepsilon} = 0$ or $m = 0$, eqn (3) reduces to a strain rate independent relation.

A finite strain version of the J_2 flow theory of plasticity in an updated Lagrangian formulation will be generalized to incorporate the thermo-elasto-viscoplastic material response. We use eqn (3) as a constitutive equation relating the representative stress $\bar{\sigma}$, representative strain $\bar{\varepsilon}$, representative strain rate $\dot{\bar{\varepsilon}}$ and absolute temperature T. The total strain rate is assumed to be the sum of the thermal, elastic and viscoplastic components:

$$d_{ij} = d_{ij}^{\mathrm{T}} + d_{ij}^{\mathrm{e}} + d_{ij}^{\mathrm{vp}}. \tag{4}$$

The thermal and elastic components are given respectively by

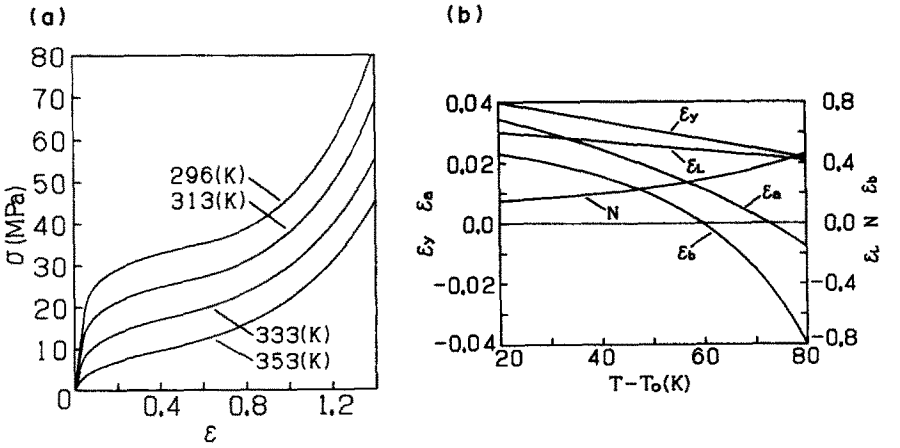

Fig. 1. Uniaxial true stress–natural strain curves for isothermal deformation (a) and temperature dependency of parameters (b).

$$d_{ij}^{T} = \alpha\delta_{ij}\dot{T}, \tag{5}$$

$$d_{ij}^{e} = \frac{1+\nu}{E}\left\{\frac{1}{2}(\delta_{ik}\delta_{jl}+\delta_{il}\delta_{jk}) - \frac{\nu}{1+\nu}\delta_{ij}\delta_{kl}\right\}\overset{\nabla}{S}_{kl}$$

$$= B_{ijkl}^{e}\overset{\nabla}{S}_{kl}. \tag{6}$$

Here, α is the thermal expansion coefficient, $(\dot{})$ denotes the material time derivative, E is Young's modulus, and ν is Poisson's ratio. $\overset{\nabla}{S}_{kl}$ denotes the Jaumann rate of the Kirchhoff stress tensor S_{kl} which is identical to the Cauchy stress tensor σ_{kl} in the current state. Next, the viscoplastic component is given by

$$d_{ij}^{vp} = p_{ij}\dot{\bar{\varepsilon}}, \quad p_{ij} = \frac{3\sigma'_{ij}}{2\bar{\sigma}}, \tag{7}$$

where σ'_{ij} is the deviatoric part of the Cauchy stress tensor. The inverse of eqn (6), together with eqns (4), (5) and (7), gives (Tomita *et al.*, 1989, 1990):

$$\overset{\nabla}{S}_{ij} = D_{ijkl}^{e}d_{kl} - P_{ij}\dot{\bar{\varepsilon}} - \beta_{ij}\dot{T},$$

$$P_{ij} = \frac{E}{1+\nu}p_{ij}, \quad \beta_{ij} = \frac{\alpha E}{1-2\nu}\delta_{ij} - \frac{1}{E}\frac{\partial E}{\partial T}\sigma_{ij}. \tag{8}$$

In eqn (8), D_{ijkl}^{e} is an elastic stiffness tensor and an inverse of B_{ijkl}^{e} in eqn (6).

Then, to increase the length of the time steps for stable computation, a forward gradient method (Peirce *et al.*, 1984) is applied which uses tangent moduli based on an estimate of the viscoplastic strain rate at a time interval between t and $t+\Delta t$. The final constitutive equation becomes

$$\dot{S}_{ij} = (L_{ijkl}^{tan} - F_{ijkl})d_{kl} - \frac{\eta}{1+\xi}P_{ij} - \dot{T}\beta_{ij},$$

$$L_{ijkl}^{tan} = D_{ijkl}^{e} - \frac{1}{h}\frac{\xi}{1+\xi}P_{ij}P_{kl},$$

$$F_{ijkl} = \tfrac{1}{2}(\sigma_{ik}\delta_{jl}+\sigma_{il}\delta_{jk}+\sigma_{jl}\delta_{ik}+\sigma_{jk}\delta_{il}),$$

$$\eta = \dot{\bar{\varepsilon}}_{t} + \theta\Delta T\frac{\partial\dot{\bar{\varepsilon}}}{\partial T} + \frac{1}{E}\frac{\xi}{h}\frac{\partial E}{\partial T}\bar{\sigma}\dot{T},$$

$$\xi = = (\theta\Delta t)\frac{\partial\dot{\bar{\varepsilon}}}{\partial\bar{\sigma}}h, \quad h = p_{kl}P_{kl} - (\partial\dot{\bar{\varepsilon}}/\partial\bar{\varepsilon})(\partial\dot{\bar{\varepsilon}}/\partial\bar{\sigma})^{-1}, \tag{9}$$

where θ is a parameter with a value of $0 \leqslant \theta \leqslant 1$. More precise discussion concerning the derivation of the constitutive equation can be found in Tomita *et al.* (1989, 1990). The simplified constitutive equation shown in eqn (9) cannot be expected to accurately describe the general history-dependent response of underlying polymeric materials. However, the constitutive equation employed can be adequate for investigating the characteristic features of the strain, strain rate and temperature-dependent deformation behavior of polymeric materials.

3. METHOD OF ANALYSIS

The numerical procedure employs the well-established finite element method (Kitagawa and Tomita, 1971, 1980), along with the constitutive equation (9). The second and

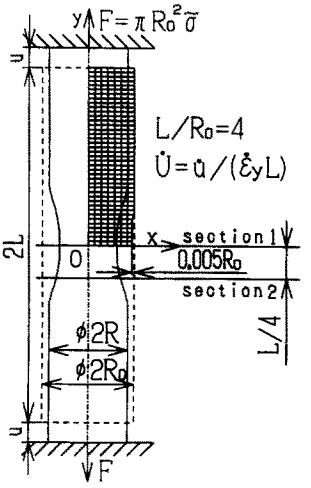

Fig. 2. Analytical model and finite element discretization. $L/R_0 = 4$, $\dot{U} = \dot{u}/(L\dot{\varepsilon}_y)$, $\bar{\sigma}$: normalized force, u: end displacement.

third terms of the right-hand side of eqn (9), which represent the strain rate and temperature-sensitive effects, respectively, are entered into the nodal force term in the finite element equation. Meanwhile, the finite-element differential heat conduction equation may be established by the weak form expression of the energy balance equation (Oden and Aguirre-Ramirez, 1969) in conjunction with Fourier's law of heat conduction. Ninety-five percent of the viscoplastic work is assumed to transform into heat. The Houbolt method [Bishop (1956), see also Bathe and Wilson (1976) for finite element analysis] is used here to transform the differential equation into a finite difference equation. Two finite element equations coupled through viscoplastic work are decoupled at each time step and are then solved in turn. Namely, the finite-element equation is solved for elasto-viscoplastic deformation during a small time interval while the temperature is held constant. Heat generation and updated geometry are introduced to the solution of the finite-difference heat conduction equation, and the current geometry, temperature, stress and so on are updated again; we then proceed to the next step. Uniform temperature distribution is initially assumed throughout the bar, and the above-mentioned computations are repeated until the required deformation has been attained. Provided that the time interval is small enough, the solution process is stable and the obtained result is accurate. A fixed time interval Δt_s is applied for analysis of the finite difference heat conduction equation, whereas the time interval Δt for the finite element equation is adjusted to Δt_s by single or multiple steps. The values of parameters used are $\theta = 1.0$, $\Delta t_s = 25/\dot{U}$ and $\Delta t < 25/\dot{U}$, where $\dot{U} = \dot{u}/(L\dot{\varepsilon}_y)$ and u, L and $\dot{\varepsilon}_y$ are shown in Fig. 2 and Table 1.

Thermo-elasto-viscoplastic analysis is performed for the bars with slight initial imperfections subjected to tension at both ends. Due to the symmetry of the deformation, half of the bar with finite-element discretization shown in Fig. 2 is investigated. Each quadrilateral shown in the vertical section consists of four crossed triangular elements. Heat generated by viscoplastic work is assumed to be discharged through convection to air at the side surface. The remaining surfaces are assumed to be adiabatic boundaries.

Table 1. Material and computational parameters.

ν	Poisson's ratio	0.3333
α	Thermal expansion coefficient	1.4×10^{-4} 1 K^{-1}
λ	Thermal conductivity	0.326 W m^{-1} k^{-1}
λ_{air}	Heat transfer coefficient	1.256×10^4 W m^{-2} K^{-1}
ρ	Density	9.4×10^2 kg m^{-3}
$\dot{U}$	Normalized rate $\dot{U} = \dot{u}/(L\dot{\varepsilon}_y)$	10, 10^3, 10^5
m	Strain rate sensitivity exponent	0.01, 0.05
$\dot{\varepsilon}_y$	Reference strain rate	2.0×10^{-5} 1 s^{-1}

For all calculations reported here, the material and computational parameters used are summarized in Table 1 and the temperature dependency of the elasticity modulus and specific heat are expressed by $E = 1045 - 10.63(T - T_0)$ (MPa), and $c = 1.55 - 25.1/(T - T_0 - 108)$ (kJ kg^{-1} K^{-1}), respectively. T is the absolute temperature and $T_0 = 273$ K is the reference temperature.

4. RESULTS AND DISCUSSION

As discussed in Section 2, uniaxial stress–strain relations of polymeric materials strongly depend on the temperature and strain rate. In quasi-static and isothermal deformation, the effect of environmental temperature, in other words, the work-hardening characteristics, substantially influences the neck propagation behavior. Otherwise, a coupled effect of the deformation-induced heating and its conduction, and material temperature and strain rate sensitivities manifest themselves in the neck propagation behavior. Here, the first part of the discussion is restricted in order to concentrate on the effect of the environmental temperature on neck propagation. Therefore, quasi-static and isothermal deformations with $\dot{U} = 10$ (corresponding strain rate is 0.0002 s^{-1}) under four different temperatures, 296, 313, 333 and 353 K, are analysed.

To clarify the effect of temperature on the global behavior of neck propagation, the load versus elongation has been depicted in Fig. 3(a). For the present case, the computations were terminated at $u/L = 1.5$ to suppress the numerical error associated with extreme elongation of the specific element. The overall deformations are essentially the same as in the literature of Neale and Tugcu (1985), except for the high temperature case (353 K). The force attains the maximum$\tilde{\sigma}_{max}$ and then it drops to the local minimum $\tilde{\sigma}_{min}$ with accompanying neck localization. Upon further straining, the neck stabilizes the neck propagation takes place under approximately steady-state conditions. From the uniaxial stress–strain relation (1), the necking and the stabilization of necking start at $\varepsilon = N + \varepsilon_a$ and ε_L, respectively. Figure 1(b) illustrates how the difference between these two strains decreses as the temperature increases. This results in the reduction of the necking stage with decreasing relative values of $\tilde{\sigma}_{max}$ with respect to $\tilde{\sigma}_{min}$. Since $\varepsilon_L < N + \varepsilon_a$ for 353 K shown in Fig. 1, unlike other cases, the corresponding deformation behavior exhibits no localization.

Figure 3(b) indicates the evolution of the radius of specimen R/R_0 at cross-section 1 and the triaxiality factor F_T. F_T is defined as the ratio of average axial stress $\tilde{\sigma}_{yy}$ to average representative stress $\bar{\tilde{\sigma}}$ through specimen cross-section, i.e. $F_T = \tilde{\sigma}_{yy}/\bar{\tilde{\sigma}}$ at cross-sections 1 and 2, shown in Fig. 2. F_T at cross-section 2 has been shown to clarify the deformation

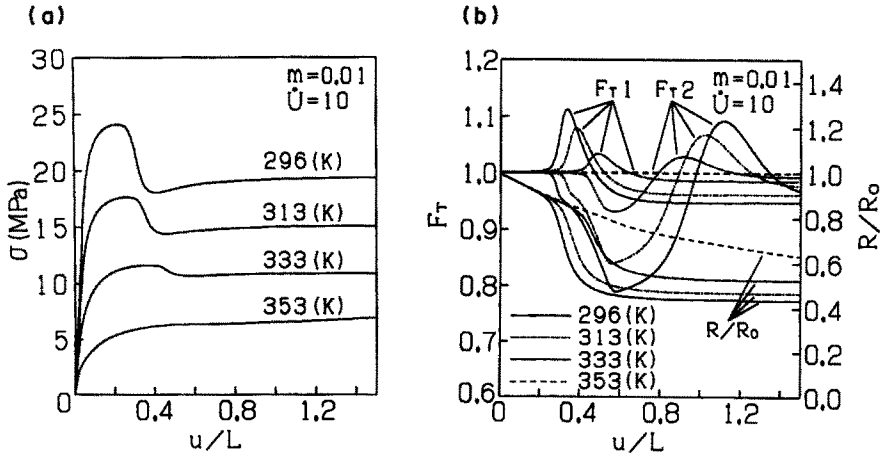

Fig. 3. Load–elongation curve (a), and evolution of triaxiality factors F_{T1}, F_{T2} at cross-sections 1, 2 in Fig. 2 and normalized radius of R/R_0 at cross-section 1 (b) for quasi-static and isothermal deformation.

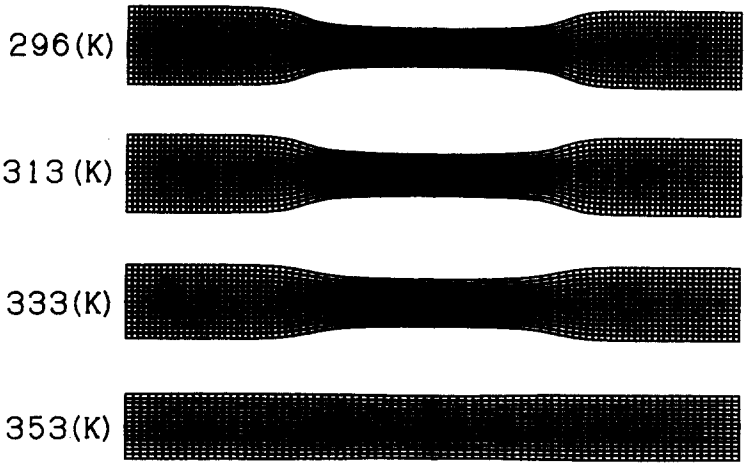

Fig. 4. Deformed specimen profiles at elongation $u/L = 0.8$ for quasi-static and isothermal deformation.

behavior at different positions in the bar. Corresponding deformation profiles at elongation $u/L = 0.8$ are shown in Fig. 4.

The relative radius of the specimen R/R_0 at cross-section 1 decreases uniformly as the deformation proceeds and then drops with neck formation. With neck propagation, it tends to a specific value. R/R_0 in Figs 3(b) and 4 suggest that the smaller-sized and more diffuse neck propagates as the temperature increases, which conforms to the reduction of necking stage.

The triaxiality factor F_{T1} at cross-section 1 suddenly increases as the load starts to drop from the maximum and attains the maximum F_{T1max} where the load drops to the local minimum. With further deformation, it decreases and asymptotically tends to the specific value F_{T1s}, which approaches unity as the temperature increases. On the other hand, due to the onset of necking at cross-section 1, the triaxiality factor F_{T2} first decreases to the minimum F_{T2min} and then increases to the maximum F_{T2max} as the neck propagates. Subsequently, it tends toward the specific value F_{T2s}. Since the deformation states are different, the two steady-state triaxiality factors have some discrepancy between them, and $F_{T1s} < F_{T2s}$ at all times. Furthermore, the triaxiality factor at the cross-section far removed from cross-section 1 behaves in much the same way as that of F_{T2}. It is noted that the stress state at cross-section 2 experiences a severer three-dimensional stress state as compared with that at cross-section 1. The delay in the onset of F_{T1max} and the decrease in magnitude of F_{T1max} in the high temperature range are strongly related to the onset of necking and the reduction of necking stage.. On the other hand, the delay in the onset of F_{T2max} in the low temperature range can be explained such that the end-displacement induced by neck propagation of unit length increases as R/R_0 decreases.

These results suggest that the material points in the deformed bars experienced at different stress history depending on their position and that special attention must be paid to the three-dimensional stress distribution to determine the uniaxial stress–strain relation, as was done by Tomita and Hayashi (1991).

Next, the effect of strain rate and temperature sensitivity on neck propagation has been investigated by thermo-elasto-viscoplastic analysis for the strain rate sensitivity parameters $m = 0.01, 0.05$ and for the nominal deformation rates $\dot{U} = 10, 10^3, 10^5$ (the corresponding strain rate is 0.0002, 0.02, 2 s^{-1}) with the material constants shown in Fig. 1 and Table 1 (Itoh *et al.*, 1980) and an enviornmental temperature of 296 K. An adiabatic response in which 95% of the viscoplastic work is converted to heat and causes a corresponding rise in temperature without heat transfer inside the specimen has also been investigated for $\dot{U} = 10$(AD) where (AD) denotes the adiabatic deformation. Since an excessive extention of the finite element mesh for $\dot{U} = 10$(AD) and $\dot{U} = 10^5$ was seen for specific elements, to

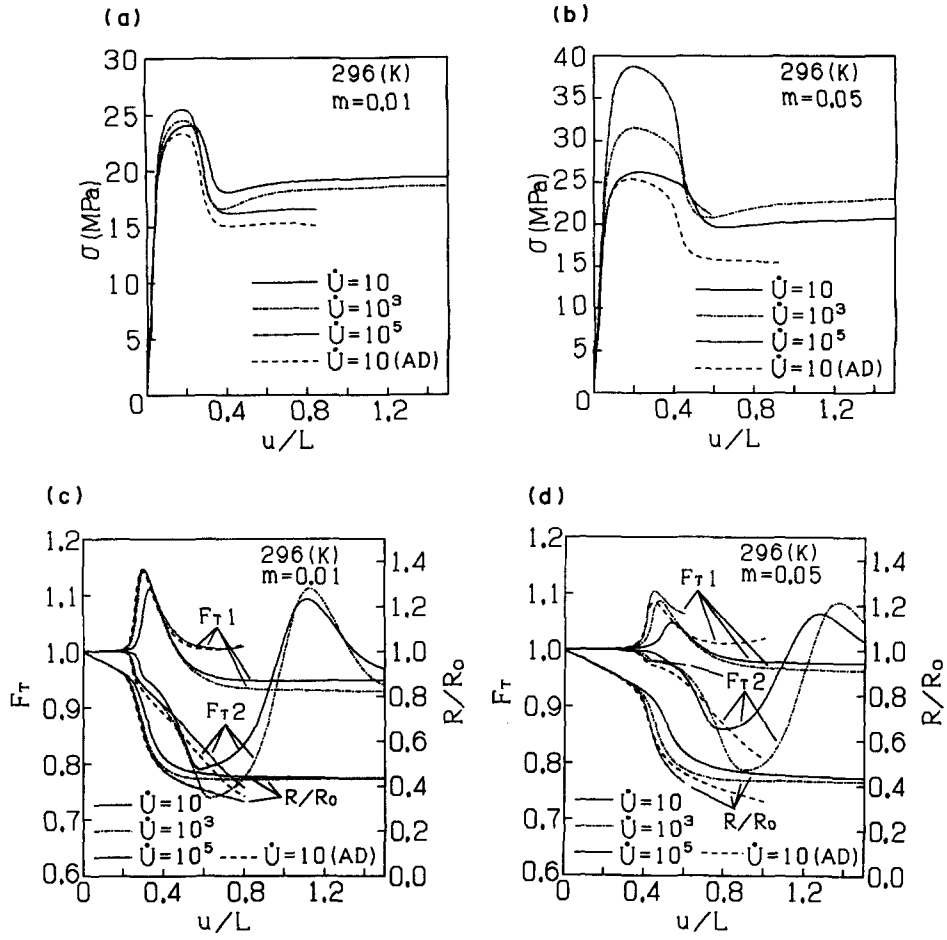

Fig. 5. Load-elongation curve (a), (b), and triaxiality factor and relative radius (c), (d) for rate and temperature dependent deformation.

avoid the introduction of numerical error, computations were terminated when the ratio of extension of two neighboring elements exceeded approximately 1.5.

Figures 5(a) and (b) show the load versus elongation, and the evolution of the triaxiality factor and the normalized radius, respectively. Figure 6 shows the natural strain–elongation curves for the element located at the origin in Fig. 2. In this figure, l_0 and l are the initial and current lengths of the element, respectively.

The results clarify that the effect of heat induced by irreversible work is rather small before the maximum load point, irrespective of the material strain rate sensitivity, and it predominantly affects the deformation behavior of the subsequent stages. From Fig. 5(a), it is noted that an increase in the deformation rate causes the parallel upward shift in the

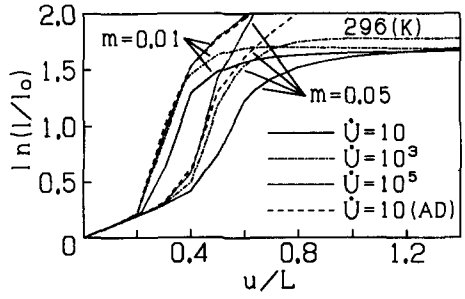

Fig. 6. Natural strain–elongation curves for the element at the origin in Fig. 2. l_0, l: initial and current length of element.

load–elongation curve at the early stage of deformation. As discussed in the strain rate dependent isothermal case of metal [Chung and Wagoner (1986); see also Tomita *et al.* (1989)], these magnitudes of shift increase as deformation rate and strain rate sensitivity m increase, whereas they may not cause a substantial change in the elongation at $\tilde{\sigma}_{max}$. The latter aspect was also noted by Tugcu and Neale (1988). The stabilization effect of the strain rate sensitivity is observed after the maximum load point where the load–elongation curves for $m = 0.05$ exhibit more gentle decreases accompanying low triaxiality factors and a diffused neck profile (Fig. 7) when they are compared with those for $m = 0.01$.

The competing effects of stabilization by strain rate sensitivity and destabilization by thermal softening are observed in the load–elongation curve where three curves for $\dot{U} = 10$, 10^3 and 10^5 cross in the necking stage. Furthermore, for high strain rate sensitivity, the strain rate hardening effect overcomes the thermal softening in the neck propagating stage. Comparison between the conductive case with $\dot{U} = 10$ and the adiabatic case with $\dot{U} = 10$(AD) clarifies the effect of heat conduction in the low rate of deformation. Results from the adiabatic case show a completely different feature from the conductive case. As we can see in Fig. 6, an extension of the element continuously increases and the corresponding deformation behavior exhibits no steady state. Consequently, thermo-coupled analysis is required to investigate the influence of the heat induced by the irreversible work and its conduction. The influence of the rate of deformation on the triaxiality factors can be

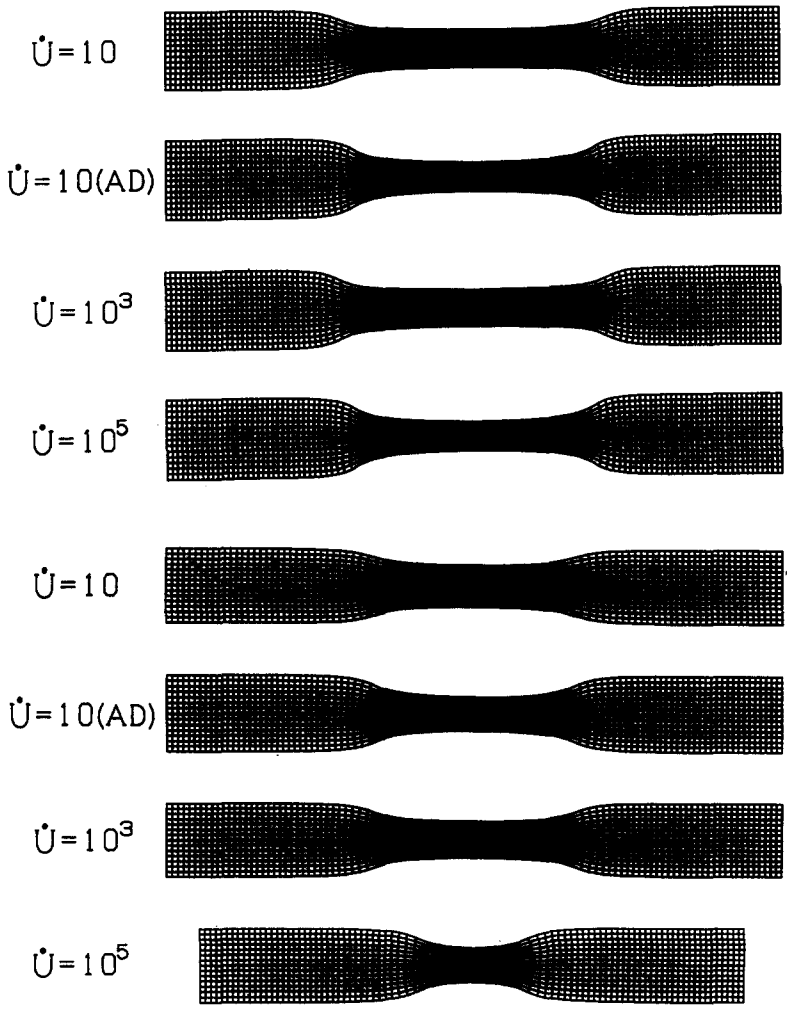

Fig. 7. Deformed specimen profiles at elongation $u/L = 0.8$ ($u/L = 0.6$ for $m = 0.05$ and $\dot{U} = 10^5$) for rate and temperature dependent deformation.

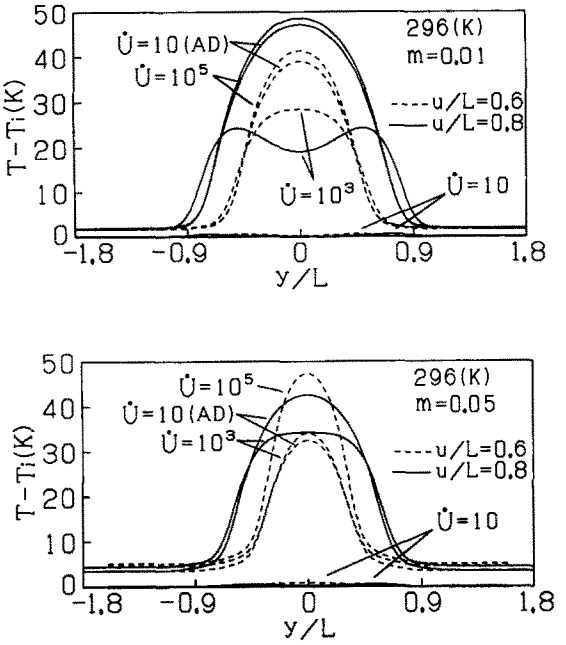

Fig. 8. Temperature rise in degree along the y-axis.

observed in their values at the later stages of deformation. Due to the destabilization effect of thermal softening, as we can see in the adiabatic case, steady-state neck propagations may not be observed in high rates of deformation.

Furthermore, computations have been performed to explore the critical temperatures under which the effect of thermal softening on neck propagation becomes insignificant, and a steady-state neck propagation occurs. The results suggest that the corresponding strain rates are approximately 0.002 s^{-1} and 0.2 s^{-1} in average strain rate, respectively, and they decrease as the material strain rate sensitivity increases. Additionally, the effect of thermomechanical coupling on the deformation behavior is substantial, especially at low deformation rates, and an assumption of adiabatic processes leads to serious overestimation of the thermal effect which causes the catastropic difference in deformation behavior.

Figure 7 shows the deformed specimen profiles and corresponding meshes for $u/L = 0.8$ ($u/L = 0.6$ for $m = 0.05$ and $\dot{U} = 10^5$) under different deformation conditions. The figure clearly depicts the characteristic feature of the steady-state and nonsteady-state deformation behaviors. Figure 8 shows the temperature rise with respect to initial temperature $T_i = 296$ K along the y-axis for different deformation stages. It clearly indicates the propagation of the heat source which in turn obstructs the local heating and causes gentle disribution of heat to the unnecked parts for relatively slow deformation. A different result can be seen in cases of a high rate of deformation and adiabatic deformation, where the high temperature area is fixed in a specific area. The subsequent deformation process manifests itself as autocatalytic. The temperature rise in Tugcu and Neale (1990) is comparable with that of the present investigation. Not knowing the values of individual material parameters, it is very difficult to make a direct comparison with the present case; however, the existence of nonsteady-state deformation may not be removed in their analysis.

5. CONCLUSIONS

The present investigation has employed a rather simple strain rate and temperature-dependent isotropic constitutive model; the results nevertheless provide insight into the effects of strain rate and temperature sensitivities and thermomechanical coupling on

the deformation behavior of polymeric material. The main results under quasi-static and isothermal deformation are as follows:

(1) The decrease in difference between the strain at the maximum load point and that of the upturn point in the uniaxial stress strain relation in the high temperature range causes the decrease in the relative value of $\tilde{\sigma}_{max}$ with respect to $\tilde{\sigma}_{min}$, size of neck, and three-dimensionality of the stress system.
(2) The triaxiality factors at the center and an off-center cross-section of the bar are generally different and the material at off-center cross-section experiences a severer three-dimensional stress state compared with that at the center cross-section.

The thermomechanical coupled analyses clarified the following:

(3) The strain rate hardening effect causes the shift in the load–elongation curve in the early stage of deformation, whereas the competing effects of stabilization by strain rate sensitivity and destabilization by thermal softening appear in the necking stage.
(4) In the high rate of deformation and adiabatic case, due to the severe thermal softening, the neck does not propagate and the heat source is fixed in a specific area. Accordingly, the deformation process manifests itself autocatalytically.
(5) In the present materials, the critical temperatures under which the effect of thermal softening on neck propagation becomes insignificant, and steady-state neck propagation occurs at approximately 0.002 s^{-1} and 0.2 s^{-1}, respectively, and they decrease as the material strain rate sensitivity increases.

Acknowledgement—This work has been financially supported in part by the Hyogo Foundation for Development and Promotion of Science and Technology, and is gratefully acknowledged.

REFERENCES

Bathe, K. J. and Wilson, D. L. (1976). Numerical methods in finite element analysis. Prentice-Hall, Englewood Cliffs, New Jersey.
Bishop, J. F. W. (1956). An approximate method for determining the temperatures reached in steady motion problems of plane strain. *Q. J. Appl. Math.* **9,** 236–246.
Chater, E. and Hutchinson, J. W. (1984). Mechanical analogs of coexistent phases. In *Phase Transformation and Material Instabilities in Solids* (Edited by M. E. Gurtin), pp. 21–36. Academic Press, Orlando, FL.
Chung, K. and Wagoner, R. (1986). Invariance of neck formation to material strength and strain rate for power–law materials. *Metall. Trans.* **A17,** 1632–1633.
Fager, L. O. and Bassani, J. L. (1986). Plane strain neck propagation. *Int. J. Solids Structures* **22,** 1243–1257.
Hutchinson, J. W., and Neale, K. W. (1983). Neck propagation. *J. Mech. Phys. Solids* **31,** 405–426.
Itoh *et al.* (Eds) (1980). *Handbook of Plastic Data.* Kogyo Chosakai (in Japanese).
Kitagawa, H. and Tomita, Y. (1971). An incremental finite element analysis of two dimensional large strain and large displacement problems for elastic–plastic materials, *Proc. 21st Japan Natl Congr. Appl. Mech.*, pp. 243–255. University of Tokyo Press, Tokyo.
Kitagawa, H. and Tomita, Y. (1980). On the finite element method for large elastic plastic strain problem. *J. Soc. Materials Japan* **29,** 663–675 (in Japanese).
Kyriakides, S. (1986). Propagating buckles in long confined cylindrical shells. *Int. J. Solids Structures* **22,** 1579–1597.
Kyriakides, S., Yeh, M.-K. and Raach, D. (1984). On the determination of the propagation pressure of long circular tubes. *Trans. ASME, J. Pressure Vessel Tech.* **106,** 150–159.
Neale, K. W. and Tugcu, P. (1985). Analysis of necking and neck propagation in polymeric materials. *J. Mech. Phys. Solids* **33,** 323–337.
Oden, J. T. and Aguirre-Ramirez, G. (1969). Formulation of general discrete models of thermomechanical behavior of materials with memory. *Int. J. Solids Structures* **5,** 1077–1093.
Peirce, D., Shih, C. F. and Needleman, A. (1984). A tangent modulus method for rate dependent solids. *Comput. Struct.* **18,** 875–887.
Tomita, Y., Asada, S. and Shindo, A. (1989). Flow localization behaviors of thermo elasto-viscoplastic block under plane strain tension. *Proc. 32nd Japan Materials Research*, pp. 302–308. The Society of Materials Science, Kyoto, Japan.
Tomita, Y. and Hayashi, K. (1991). Deformation behavior in elasto-viscoplastic polymeric bars under tension. *Proc. Plasticity* '91, pp. 524–527. Elsevier Applied Science.
Tomita, Y., Shindo, A. and Sasayama, T. (1990). Plane strain tension of thermo-elasto-viscoplastic blocks. *Int. J. Mech. Sci.* **32,** 613–622.
Tomita, Y., Takahashi, T., and Shindo, A. (1990). Neck and bulge propagation in polymeric cylinders. *Int. J. Mech. Sci.* **32,** 335–343.
Tugcu, P. and Neale, K. W. (1987a). Necking and neck propagation in polymeric materials under plane strain tension. *Int. J. Solids Structures* **213,** 1063–1085.
Tugcu, P. and Neale, K. W. (1987b). Analysis of plane-strain neck propagation in viscoplastic polymeric films. *Int. J. Mech. Sci.* **29,** 793–805.

Tugcu, P. and Neale, K. W. (1988). Analysis of neck propagation in polymeric fibers including the effect of viscoplasticity. *Trans. ASME, J. Engng Mater. Tech.* **110,** 395–400.

Tugcu, P. and Neale, K. W. (1990). Cold drawing of polymers with rate and temperature dependent properties. *Int. J. Mech. Sci.* **32,** 405–416.

Tugucu, P., Neale, K. W. and Lucero, A.-M. (1991). Effect of deformation-induced heating on the cold drawing of polymeric films. *Trans. ASME, J. Appl. Mech.* **113,** 104–111.